University of Southern Indiana
Pott College of Science, Engineering, and Education
Engineering Department
8600 University Boulevard
Evansville, Indiana 47712

Rehabilitative Design & Structural Health Monitoring of New Harmony Bridge

Cole Butler, Jared Scales
ENGR 491 – Senior Design
Fall 2021

Photo courtesy of WJE Associates, Inc.

Approved by: _____
Faculty Advisor: Kerry Hall, Ph.D. Date

Approved by: _____
Department Chair: Paul Kuban, Ph.D. Dat

Acknowledgements

In this section, we would like to acknowledge Dr. Adam Tennant and Dr. Kerry Hall, our two faculty advisors, Adam Dauby for providing instructions and assistance with the STS4 system by BDI, Department Head Dr Paul Kuban, department secretary Ms. Jamie Curry, Mark Logel in risk management, Mr. Rodney "Rod" Clark and Dr. Ron Eimer on the New Harmony Bridge Authority, and Claire Eagle and Paul Goodman with the New Harmony Atheneum.

Abstract

This project analyzes the structural design of the New Harmony Bridge and suggests a redesign of the deck in order to meet modern standards. The New Harmony Bridge (opened in 1930) holds a significant historic value which attracts a high public interest. The age of the bridge is again reinforced in the unique structural elements such as rolled Carnegie steel shapes throughout the bridge and its use of the K truss. Sensors were strategically placed on the bridge to measure short-term moving loads over multiple tests. These results provide insight as to how the structure reacts to different load cases which is useful considering the bridge has been out of commission since 2012. More specifically, these tests explore any load sharing capabilities the beams may have. Additionally, a conceptual design for the repaired concrete deck was developed using shear studs to achieve a composite beam design. This included 2D models in RISA to determine demand and analyses in Microsoft Excel to determine capacity. The overall goal is for the redesign to withstand the loading of an HS-20 per AASHTO code.

Table of Contents

1.0 REHABILITATIVE DESIGN AND STRUCTURAL HEALTH MONITORING

1.1 BACKGROUND

The project was selected due to its local impact and historical relevance. The New Harmony Toll Bridge is a two-lane bridge across the Wabash River that connects Illinois Route 14 with Indiana State Road 66. It links White County, Illinois with Posey County, Indiana. When erected on May 1, 1928, the New Harmony Toll Bridge was the first highway bridge to cross the lower Wabash River. It was constructed by the Big Wabash Bridge Company located in Carmi, Illinois. The Nashville Bridge Company located in Nashville; Tennessee was contracted as well. On December 21, 1930, the bridge was officially opened to the public.

1.2 SCOPE

Included within the scope of this project are two tests. One being the short-term moving live-load test. The other was a six-and-a-half-day test monitoring naturally occurring events that have affected the health of the bridge. Included in the scope is a short-term moving test load with both team members walking across 40-foot span of each stringer and doing a "heel-drop" movement. The data for this was analyzed to verify that the stringers shared loads.

The project has two primary software elements. AASHTO HS-20 load is the proposed demand and was tested with 2 different models in RISA 2D. STS View and STS Live were used when analyzing load sharing capabilities. While some additional models from AASHTO ware and SAP were provided by WJE and Associates, they were not used in the load sharing on the Indiana approach or the composite beam design. The new proposed design was computed in excel, using moment capacity suggestions from AISC 7th Edition, AISC Properties for Carnegie Steel Sections, AASHTO LRFD Bridge specifications 6th edition, and Structural Steel Design by McCormac & Csernak. Both members thoroughly checked one another's work while analyzing the RISA model and the Excel computation.

Additionally, resource connection seemed to be a long duration of the process. Dr Adam Tennant found contact info Dr Ron Eimer, while Cole Butler remained in correspondence with Eimer throughout the summer months. Several site visits and a stakeholder meeting of June of 2021 established the relations that made the project possible. Mark Logel corresponded with both team members and Dr Tennant and established the access agreement with the New Harmony Bridge Authority that made site visits possible. Additionally, Jared Scales navigated correspondence with Claire Eagle and Paul Goodman with the New Harmony Atheneum. This was integral for finding a place to safely store the data laptop and base station for performing a six-and-a-half-day long test for structural health monitoring.

Figure 1.1 shows a breakdown of the resulting subsystems considered.

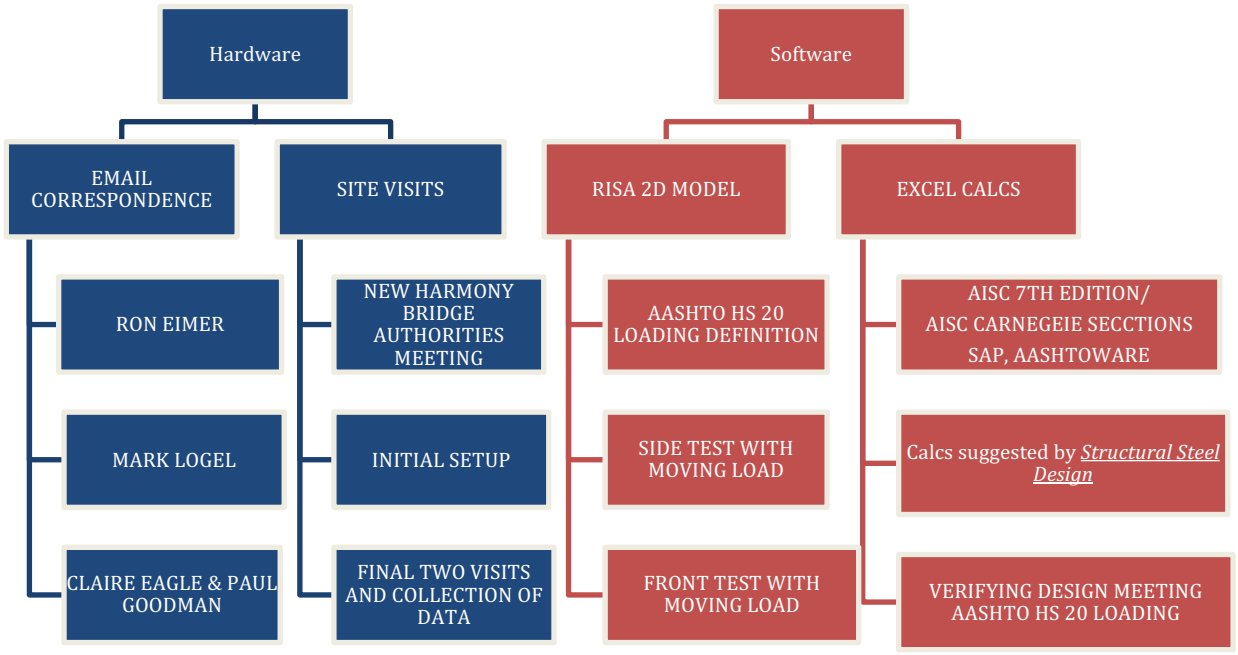

Figure 1.1: Subsystem Breakdown

The first site visit involved the two team members, Dr Hall, Rod Clark, and Dr Eimer. This meeting set out the basic guidelines on testing locations, design areas of interest, and setting up a power source for the Structural Health Monitoring test.

The second site visit involved both team members and Dr Hall. This was additional practice and testing with the strain gauge and accelerometer. This was also important for testing the range capability for the base-station at the New Harmony Athenium. This meeting was integral for practicing for the long-term structural test and creating a plan of execution for the sensors system.

The third site visit included the installation for the long-term tests. The United States Geological Survey (USGS) was gracious enough to provide power for the node for the structural health test. The instruments were also secured and electrical tape to prevent damage due to weather. Bungee cords were used to secure the node laterally, while a tub and a few wood planks were used to ensure that the node would not be submerged in a rain event. Lastly, the base station and laptop were set at the athenium with their respective power sources.

2.0 LOCAL HISTORY

2.1 Unique Architecture

The bridge has a unique design that brings interest. It is constructed as a Pratt Truss with midspan joints being constructed as K-Trusses. The two components being integrated simultaneously, and the historic nature of K-Trusses in the United States brings interest in restoration of the bridge.

2.2 Cultural Impact

As an attempt of a Utopian Community, New Harmony's historical relevance also has cultural importance that brings early education instructors and students for field trips. New Harmony is a hub for recreational activities and tourist attractions. Attractions such as the roofless church, New Harmony Athenium Museum, Labyrinth State Memorial, Harmonie State Park, and variety of restaurants and taverns draw people in from out of town. Yearly events such as the Kunstfest and Arts in Harmony events also attract people from surrounding areas. The tourism industry is an integral part of New Harmony's local economy, and the toll portion is an integral part to the economy of White County, IL. The large amount of outdoor activities present is a factor that promotes and encourages public health and social welfare, while also financially benefiting Illinois.

2.3 Networking

Due to the historical significance of the bridge, communication and networking were of the utmost importance for this project. Much of the beginning stage was spent collecting contact information and moving from person to person to gain access to the bridge so that sensors could be attached. During the conception of the project, a news article regarding the New Harmony Bridge was used to track down Wiss, Janney, Elstner Associates, Inc. as contributors to the work being done. They helped to establish contact with Ron Eimer, who happens to be both a civil engineer and a lawyer. Ron possesses an immense amount of knowledge and helped to refine the scope. He also granted the opportunity to attend a meeting in Carmi, IL between both the Indiana and Illinois Bridge Authorities where the project was discussed and approved. Over the remaining summer months, USI was in contact with both Authorities to create the *New Harmony Way Bridge Temporary Access Agreement* and the *Harmony Bridge Waiver* for those who would be accessing the bridge. Mark Logel, the Director of Risk Management at USI, took the lead in communicating between both parties and completed the documents quickly so that work could begin. Throughout the testing phase, both Ron and Rod Clark, President of the Illinois Bridge Authority, made appearances offering general guidance and advice for testing.

2.4 Media

Conversations with locals made it apparent that the bridge was deeply rooted in the town of New Harmony and part of its identity. It was clear that public interest was high, and media would play a part in the project. Trisha Lopez, a reporter for the Posey County News, reached out early on and joined one of the multiple site visits. She observed the setup for long term structural health monitoring and held individual conversations with all project members (as well as Ron Eimer) to gain a better understanding of the work being done. On October 5, 2021, the news article became publicly available and featured the project on the front page.

3.0 CURRENT CONDITIONS

3.1 Truss, Deck, and Expansion Joints

Preceding this project, WJE has concluded that the uniquely structured truss is highly functional. One of the main areas of concern is the concrete deck. There is deterioration on both sides of the bridge. The Illinois approach contains noticeably more severe damage than the Indiana approach due to the Illinois side having less of a slope and over-treatment for snow and ice deposits during the winter. This issue not only effects the concrete deck but also damages the expansion joint that are at 40-foot increments. Proper treatment and installation of gutters near the curb should mitigate future deterioration. Additional sheltering methods around expansion joints may be considered as well.

3.2 Carnegie Beams

The main area of concern is the Carnegie Beams. While the stringers presented adequate capacity at the time of the bridge's conception, they are currently not up to date with modern loading. The loading analysis that the new design will be targeting is AASHTO HS-20 loading. Additionally, a factored pedestrian load of 100 psf is considered. In addition, there are some areas near the Indiana approach where deterioration is present that should have rehabilitation in consideration.

3.3 Girder System and Meander Belt

Lastly, the plate girder system on the Illinois approach should also be considered for rehabilitation. The girder system was implemented recently when a pier needed to be removed due to scour. It scoured at a rate that was quicker than anticipated due to meandering of the river. Sediment deposits over time have pushed the flow of the river towards the Illinois side. The meandering has become so sever that it has created an oxbow lake on the Illinois side. In addition to the formation of the oxbow lake, attempts at setting riprap to stop or slow the meandering of the river have also failed. Since the meandering of the river will be a major issue on the Illinois side for a long time, it is critical that this portion gets restored. While this was an important facet to the project and one that the team had interest in, learning some of the finite element models such as SAP and AASHTOWare were difficult to integrate with the composite beam design and load sharing tests.

4.0 DEMANDS OF MODERN LOADING

In order to redesign the bridge, modern loading standards must first be established. Three main load cases were analyzed: HS-20, Pedestrian, and Staggered Pedestrian. All of these were applied to models within RISA 2D in order to read maximum bending moments, the greatest of which will be the standard for redesign. Cross section models of the bridge simulate moments carried by the bridge deck while side views of the bridge simulate moments carried by the floor beams. Since the side view models focus on the floor beams, considerations must also be made for the difference in weight between Carnegie shapes and the difference in effective base between middle and edge beams.

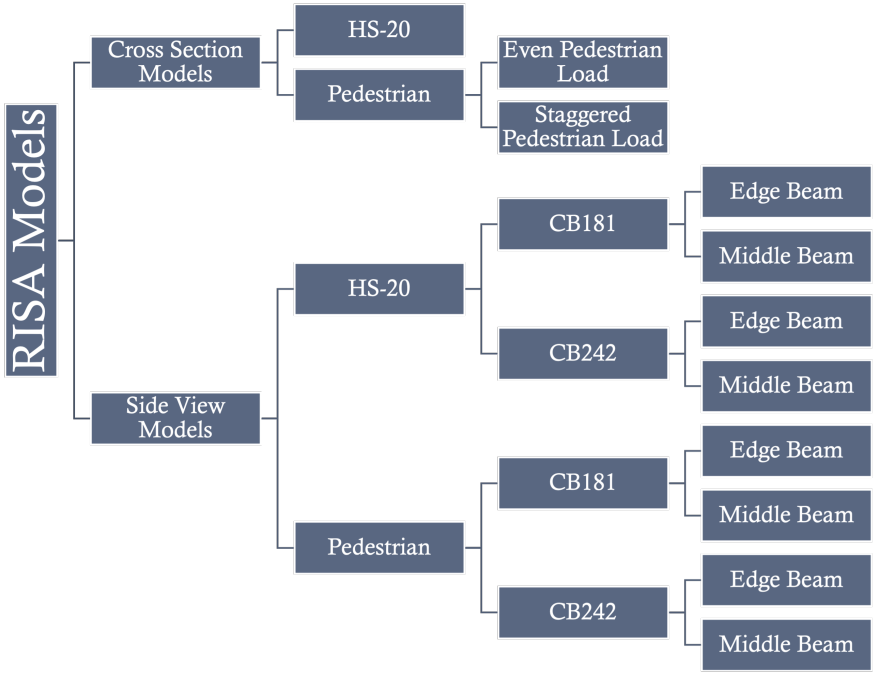

Figure 2.1: Breakdown of Load Cases for Both Models

4.1 RISA 2D Model Information

RISA 2D was the software used to develop models of the bridge, apply theoretical load cases, and read results. Two different model views were created in order to simulate moments carried by the bridge deck and floor beams, those being cross sectional view and side view.

The Cross Section Model shows the moment carried by the bridge deck. The length of the model extends across all five floor beams until the middle of each curb. This results in a length of 20.75 ft. The width of the model is 14 ft which accommodates the greatest distance between HS-20 truck axles.

The Side Model shows the moment carried by the floor beams (stringers). The length for all side models is 40 ft which covers an entire span. The "Middle" and "Edge" beam scenarios will have differing widths due to the difference in effective base between them. Middle beam models will have a width of 4.5 ft while the edge beam models will have a width of 3.875 ft.

4.2 Load Cases

4.2.1 Dead Load

The Cross Section Model includes the dead load of the concrete deck and the concrete curbs. RISA 2D automatically calculates the self-weight of the concrete using 4000 NW concrete and a 7 in deck thickness. The dead weight of the curb was calculated using an approximated area of 54 in^2 and assuming a weight of 150 lb/ft^3 which is the standard concrete weight. This results in a weight of 4.6875 lb. each curb which will be present twice in the model, once at each end.

The Side View Model includes the self-weight of the floor beams themselves. Since they are Carnegie shapes with unique properties, the *Carnegie Steel Manual* was referenced for these values. According to the

manual, the CB242 shape has a self-weight of 76 plf while the CB181 shape has a much smaller self-weight of only 47 plf.

Section Index	Depth of Section, Inches		Weight per Foot, Pounds	Flange Width, Inches		Flange Thickness, Inches		Web Thickness, Inches	
	Decimal	Fraction		Decimal	Fraction	Decimal	Fraction	Decimal	Fraction
	24.308	24 5/16	94	9.844	9 27/32	0.817	13/16	0.499	1/2
CB 242	24.154	24 5/32	85	9.797	9 51/64	0.740	47/64	0.452	29/64
	24.000	24	76	9.750	9 3/4	0.663	21/32	0.405	13/32
CB 241	24.000	24	70	8.500	8 1/2	0.663	21/32	0.400	13/32

Figure 4.1: Self-Weight of CB242

Section Index	Depth of Section, Inches		Weight per Foot, Pounds	Flange Width, Inches		Flange Thickness, Inches		Web Thickness, Inches	
	Decimal	Fraction		Decimal	Fraction	Decimal	Fraction	Decimal	Fraction
	18.242	18 15/64	78	8.565	8 9/16	0.866	55/64	0.471	15/32
CB 182	18.110	18 7/64	72	8.530	8 17/32	0.800	51/64	0.436	7/16
	18.000	18	67	8.500	8 1/2	0.745	3/4	0.406	13/32
	18.252	18 1/4	58	7.573	7 37/64	0.676	43/64	0.393	25/64
CB 181	18.114	18 7/64	52	7.534	7 17/32	0.607	39/64	0.354	23/64
	18.000	18	47	7.500	7 1/2	0.550	35/64	0.320	5/16
	*18.024	18 1/32	51	7.555	7 9/16	0.562	9/16	0.375	3/8

*Special Section Web Thickness 3/8".

Figure 4.2: Self-Weight of CB181

4.2.2 HS-20 Load

The HS-20 load case that is used for both models is AASHTO defined. Figure 4.3.1 displays the side view of this load case which includes three point loads, one for each axle, at magnitudes of 8, 32, and 32 kips moving from the front axle to the rear. The spacing between the first and middle axle is 14 ft and while the spacing between the middle and rear axle can vary from 14-30 ft, 14 ft was used since this closer spacing will produce a greater bending moment when applied to the model. Figure 4.3.2 displays the rear view of the load case. This includes two point loads of 16 kips for each axle at a spacing of 6 ft. This is using the greatest point load from the side view, 32 kips, and dividing it between both axles. Figure 4.4.1 and Figure 4.4.2 show this load case applied to the RISA 2D models.

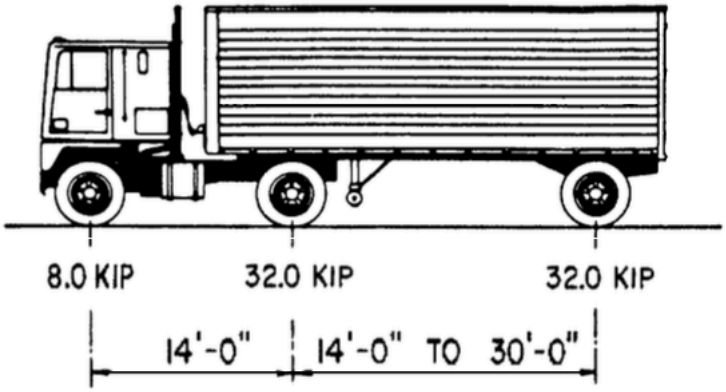

Figure 4.3.1: Side View of HS-20 per AASHTO

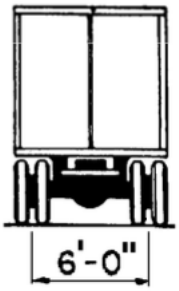

Figure 4.3.2: Rear View of HS-20 per AASHTO

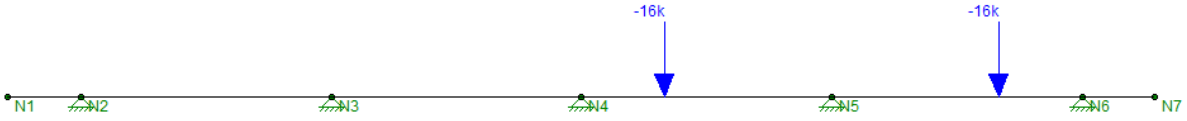

Figure 4.4.1: Cross Section View Model of HS-20 Load Case

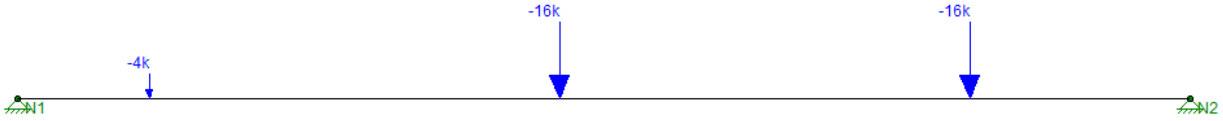

Figure 4.4.2: Side View Model of HS-20 Load Case

4.2.3 Pedestrian Load

The Pedestrian Load is assumed to be 100 psf, or 0.1 ksf, throughout. In order to translate this to units of kip/ft, it must be multiplied by the width of the model. Since the Cross Section View Models use a width of 14 ft consistently, this results in a distributed load of 1.4 kip/ft. However, the Side View Models include two different widths due to the edge beams having a shorter effective base than the middle beams. This results in a distributed load of 0.388 kip/ft for the edge beam and 0.45 kip/ft for the middle beam.

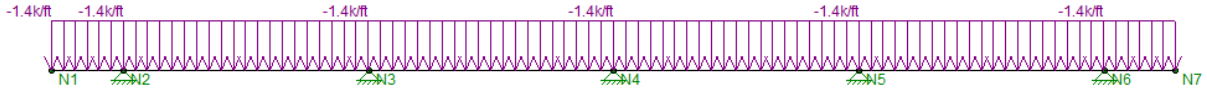

Figure 4.5.1: Cross Section View Model of Pedestrian Load Case

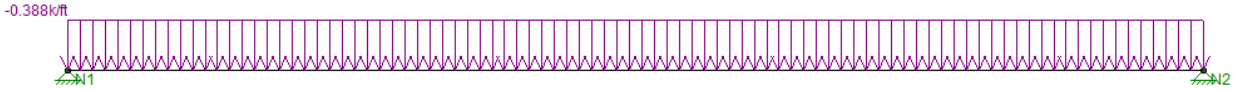

Figure 4.5.2: Cross Section View Model of Pedestrian Load Case for Edge Beam

Figure 4.5.3: Cross Section View Model of Pedestrian Load Case for Middle Beam

4.3 Cross-Section View Model Results

Three load cases were applied to the Cross Section View Model: HS-20, Pedestrian, and Staggered Pedestrian. The HS-20 load case results in a maximum bending moment of 38.3 k-ft (Figure 4.6.1). The Pedestrian load case results in a maximum bending moment of 8.1 k-ft. The Staggered Pedestrian load case resulted in a slightly higher maximum bending moment of 9.4 k-ft. While the Staggered Pedestrian load was higher than the Pedestrian load, it still was well under the demand of the HS-20 load. This means that the maximum bending moment the deck would have to withstand is 38.3 k-ft.

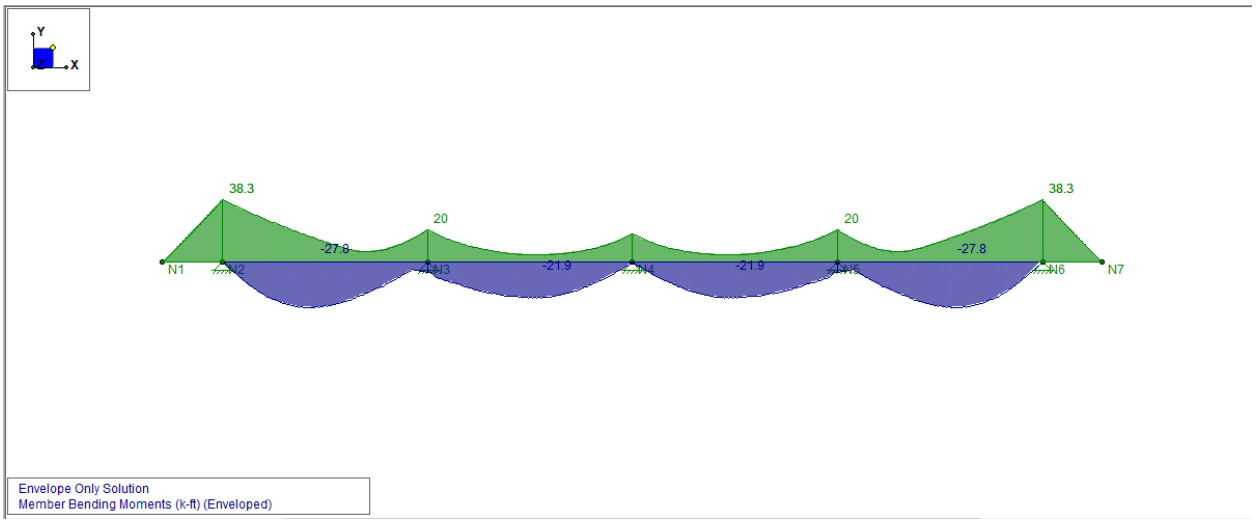

Figure 4.6.1: Cross Section Model Results – HS-20 Load Case

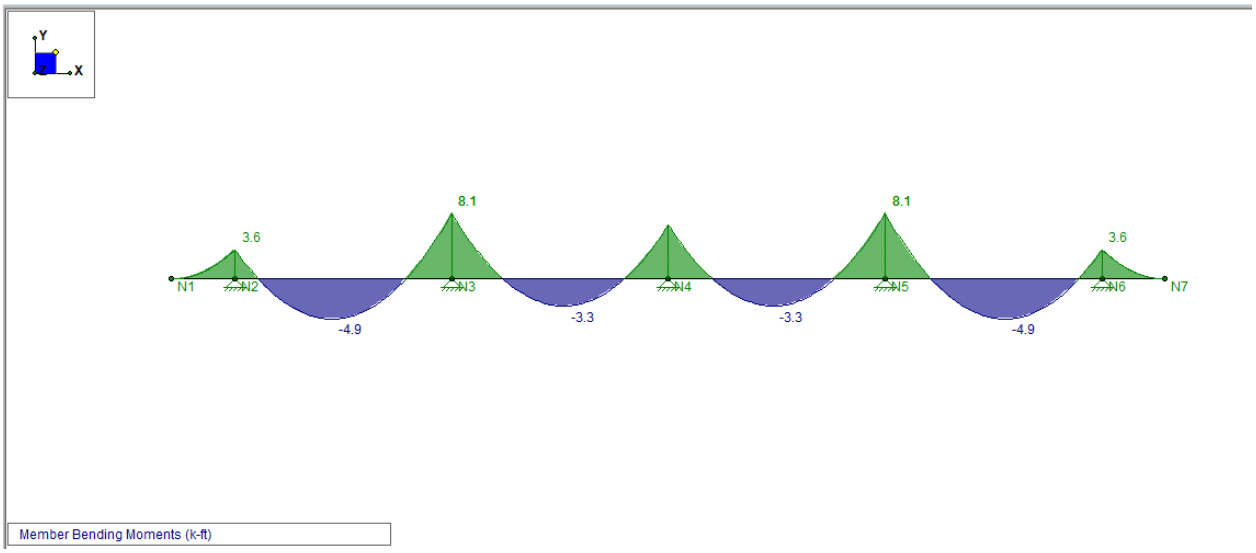

Figure 4.6.2: Cross Section Model Results – Pedestrian Load Case

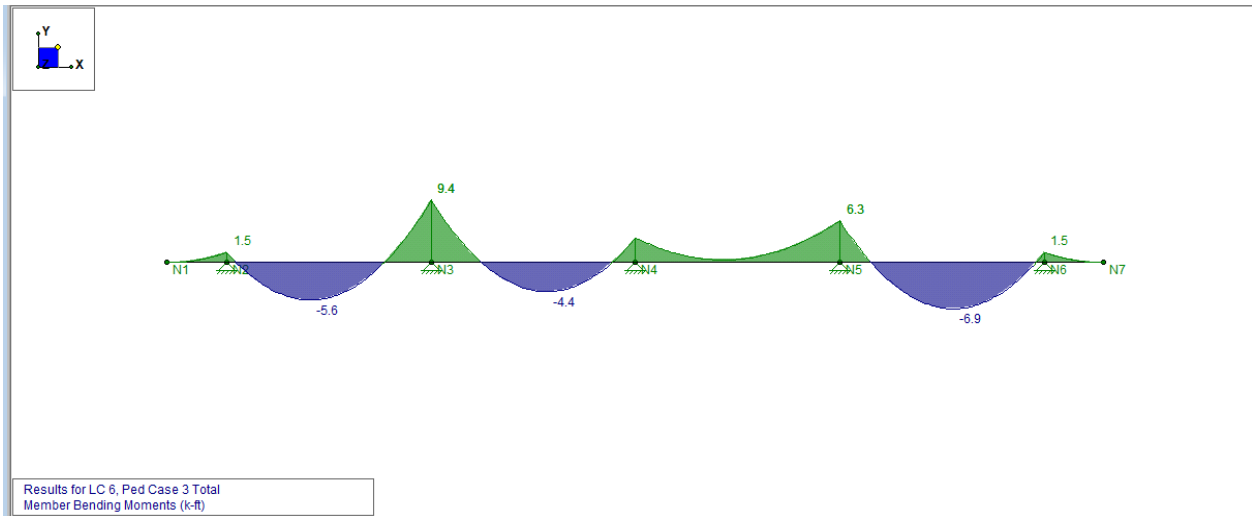

Figure 4.6.3: Cross Section Model Results – Staggered Pedestrian Load Case

4.4 Side View Model Results

For the Side View Model, only the HS-20 and Pedestrian load cases were applied. Since the Side View Model had to be slightly altered to accommodate both Carnegie shapes as well as middle and edge beams, only the model with the greatest maximum bending moment is included since that is the scenario that will be controlling. In this case, the middle CB242 model resulted in the highest bending moments for each load case. The HS-20 load case (Figure 4.7.1) results in a maximum bending moment of 530.3 k-ft while the Pedestrian load case (Figure 4.7.2) results in a maximum bending moment of 295.9 k-ft. Just as in the Cross Section View Models, the HS-20 loading is the highest demand. This means that the maximum bending moment the floor beams would have to withstand is 530.3 k-ft.

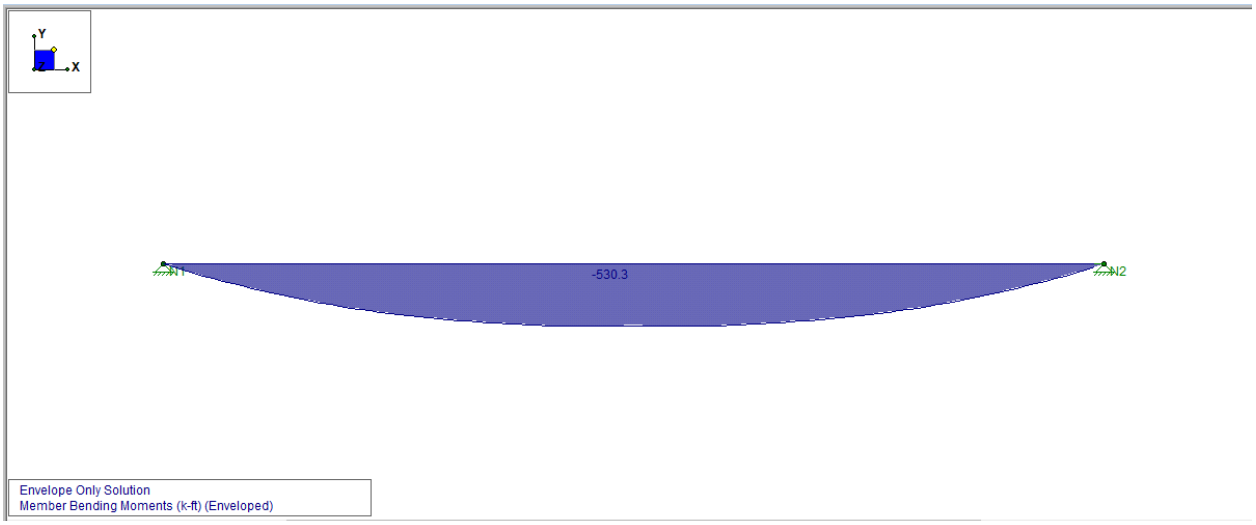

Figure 4.7.1: Side View Model of HS-20 Load Case – Controlling Scenario (Middle CB242)

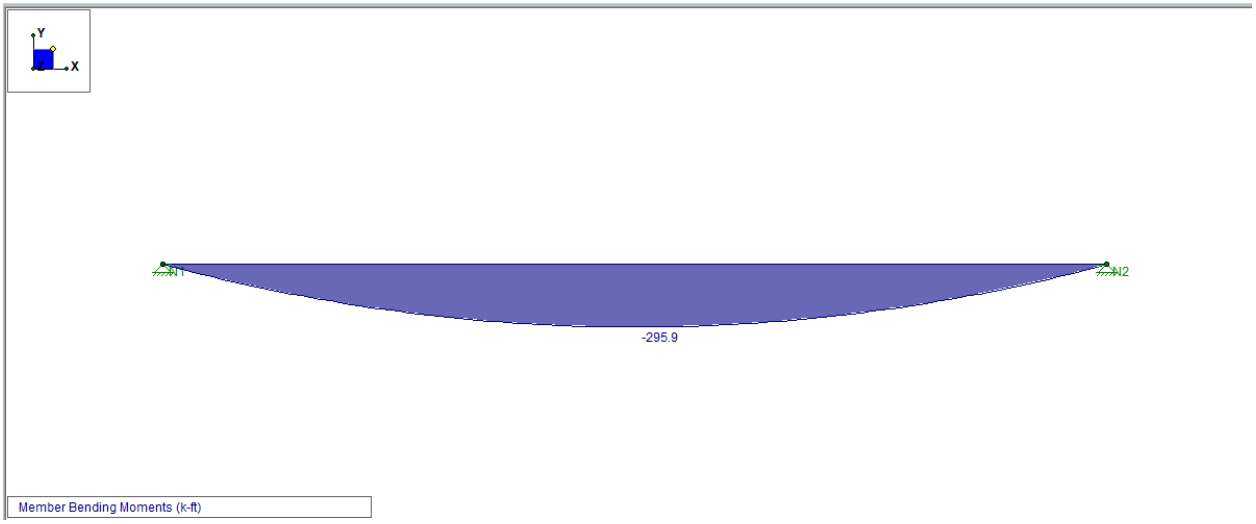

Figure 4.7.2: Side View Model of Pedestrian Load Case – Controlling Scenario (Middle CB242)

5.0 CAPACITY OF DECK REDESIGN

5.1 COMPOSITE BEAM DESIGN

The suggested design provided by liaison Ron Eimer was a composite beam design shown in the image below. This is achieved by welding shear studs into the floor beams that will go into the new layer of concrete. The first step was checking the inelastic condition. For the deformation to be considered inelastic, it must meet the condition in the equation below. *E* is modulus of elasticity for steel (29,000 ksi) , f_y is the yield strength of Carnegie steel (36 ksi), h is the height of the flange, and t_w is the web thickness. The height, flange thickness, and depth of the beam can be found in the AISC Properties for Carnegie Beam Sections.

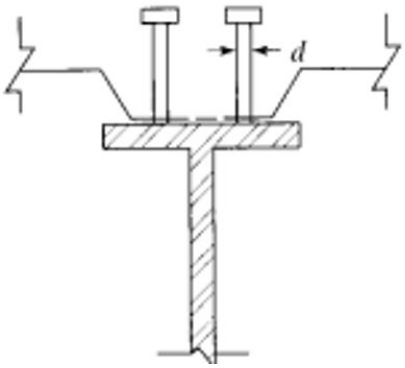

Figure 5.1: Composite Beam Diagram (*Structural Steel Design*)

$$\frac{h}{t_w} \leq 3.76\sqrt{E/f_y}$$

Equation 5.1: Inelasticity Condition (*AISC 16.94)*

Once the condition is established as inelastic with each of the respective Carnegie Sections, the next step is determining the depth of compressive strength in the concrete (a). It is found from the equation shown below. A_s is the effective area of steel, which is the cross-sectional area of the Carnegie Section, f'_c, is the design strength of concrete (4000 psi) and the b_e is the effective base. There are two effective bases that had calculated capacities. The three interior Carnegie Sections shared a capacity, while the outer two shared a capacity. This is due to effective base varying. The effective base is less than on the exterior beams since it only covers the distance to the exterior and halfway to the next beam on the opposite side (46.5 inches), while the interior effective base cover halfway to the next beam in both directions (54 inches).

$$a = \frac{A_s f_y}{.85(b_e)f'c}$$

Equation 5.2: Depth for Compressive Strength (*Structural Steel Design*)

Once a is determined, in elastic moment capacity is calculated with a, the depth of the beam (d), and the thickness of the layer of concrete (t).

$$M_n = A_s f_y(\frac{d}{2} + t - \frac{a}{2})$$

Equation 5.3: Moment Capacity (*Structural Steel Design*)

This returns a moment capacity in k*in, which for practicality purposes is converted to k*ft. It is also controlled by a factor of φ OF .85, as required for LRFD design by AISC 14th edition. This factored capacity is compared to the demand capacity for AASHTO HS-20 Loading performed in the RISA 2D model.

5.2 SHEAR STUDS

The shear transfer Q_n is governed by equation 4, where A_{sc} is the are of the shank of the shear stud, and E_c is the modulus of elasticity of concrete. The modulus of elasticity for concrete is shown by equation 5, where w is unit weight of concrete and f'_c is inputted in pounds instead of kips.

$$.5(A_{sa})\sqrt{E_c f'_c} \leq (A_{sa})R_G R_P f_U$$

Equation 5.4: Shear Transfer Governing Equation (*AISC 14th edition/ Structural Steel Design)*

$$E_c = w^{1.5}\sqrt{f'_c}$$

Equation 5.5: Modulus of Elasticity for Concrete (*Structural Steel Design)*

The minimum of the two values is considered for a design Q_n to select from in AISC 14th Edition table 3-20. Once that is determined, the shear capacity and tensile yielding of steel are needed to determine the number of studs. The minimum of these two are used to determine the number of studs. The shear is found in AISC 14th Edition, section I31-a.

$$T = A_s f_y$$

Equation 5.6: Tensile Yielding (Steel)

$$V' = .85 f'_c A_c$$

Equation 5.7: Shear Capacity (Concrete)

Tensile yielding controls the number of shear studs. The value of tensile yielding in kips determined in equation 6, divided by the shear transfer determines the number of studs per member. The minimum shear transferred is determined in Equation 4. Similar values are listed in AISC 14th edition table 3-20. The number of strong studs per rib and the diameter of the shank of the shear stud determine the transferred shear in the member. $5/8^{th}$ inch diameter with two studs in the rib presented 18.3 k, which exceeds the value of 12.38 determined by equation 4. Lastly, a simple calculation is run for spacing. As suggested by *Structural Steel Design,* 6 times the diameter of the shank is the minimum vertical spacing, while 4 times the diameter is the minimum horizontal spacing. The horizontal spacing is easily met, while the spacing of required shear studs fits in approximately ¼ of the overall span.

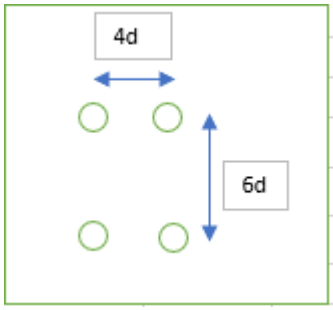

Figure 5.2: Spacing of Shear Studs as suggested by *Structural Steel Design*

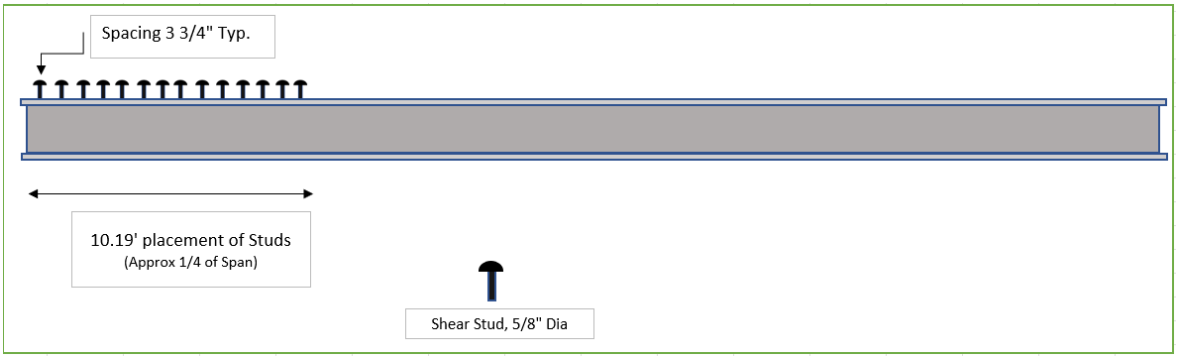

Figure 5.3: Carnegie Beam Diagram with Shear Studs

5.3 REBAR CAGE DESIGN

The first step in cage design is determining a viable reinforcement ratio (**r**) to use. This number is important in determining the amount of reinforcement steel placed within the slab to improve survivability but improve ductility of the slab. The two expressions that determine reinforcement ration on the following page.

$$\rho_{max} = .85\beta_1 \frac{f'_c}{f_y} \frac{3}{8}$$

$$\rho_{min} = MAX\left\{\frac{3\sqrt{f'_c}}{f_y}, \frac{200}{f_y}\right\}$$

Equations 5.8-9: Reinforcement Ratio Bounds (*ACI 318.14*)

The bounds for reinforcement ratio are .00333 and .01806. The reinforcement ratio can next be used to estimate the area of steel within the slab. The equation for area of steel is shown below.

$$A_s = \rho b d$$

Equation 5.10: Area of Steel Demand

Once area of steel is determined, a size of bar and number of bars for each layer can be selected. The top layer of steel will have a lower need for bars. Since AASHTO bridge specifications requires a 1 ½ inch cover at the top layer opposed to 1 inch of bottom cover, the resulting moment caused by the effective depth will be smaller. The effective base (b_e) provided by AASHTO is 14'. This is necessary again for determining the depth for compressive strength (a). Both effective base and depth of compressive strength are needed to calculate the factored moment capacity, along with the Area of the Steel and a safety factor of **F** being .90 as prompted by AISC 14th edition. The equation for factored moment capacity is shown below. Note that if using pounds for f_y for the units.

$$\emptyset M_n = \emptyset A_s f_y (d - \frac{a}{2})$$

Equation 5.11: Factored Moment Capacity for Steel Cage (*ACI 318.14)*

The final design includes No. 5 bars spaced at 8 inches on the top layer and 10 inches at the bottom layer. This gives a capacity of 147.3 k' for the top layer of steel and 129.5 k' for the bottom layer respectively. Both are over the necessary capacity for pedestrian and AASHTO HS-20 loading. The top layer is designed to resist a higher capacity and absorb the larger bending moment of the two layers, which prompts less of a demand for bars and a higher spacing. Lastly, the spacing and cover constraints per request of AASHTO must be met. The spacing must be at least 1.5 times the diameter of the selected bars. At most it is 18 inches. We found that spacing the top steel at 8 inches and bottom steel at 10 inches would meet this capacity. The top layer and

bottom layer are space vertically at 2.88 inches. This not only meets the minimum requirement for AASHTO, but also meets the top and bottom cover requirements of 1.5 inches for the top and 1 inch for the bottom layer. A figure summarizing the specs is shown below.

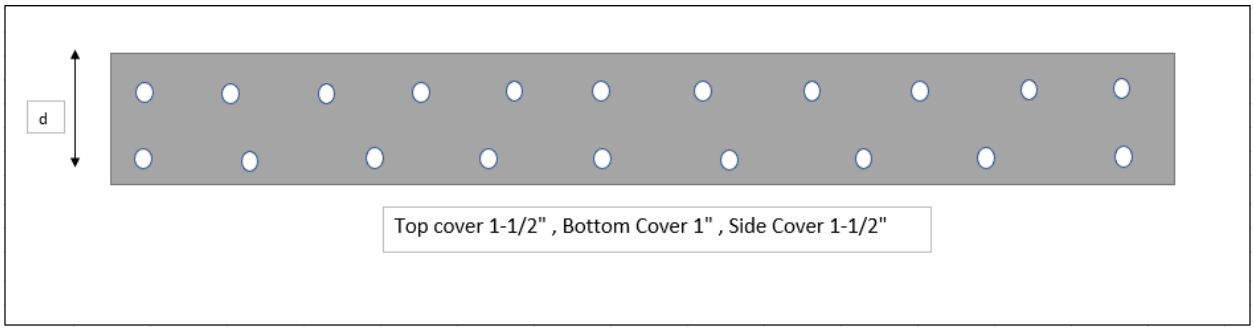

Figure 5.4: Concrete Deck and Proposed Rebar Cage Installation

6.0 LOAD SHARING CAPABILITIES

Following the redesign of the deck to withstand modern demand, a test was performed to explore the load sharing capabilities of the floor beams. This test was conducted using the STS4 by BDI along with its accompanying software, STS Live. The tests return strain data that can be used to numerically approximate the fraction of the total load experienced by each sensor's corresponding floor beam.

6.1 STS4 (Structural Testing System 4) by BDI

The Structural Testing System 4 (STS4), provided to the University courtesy of BDI, consists of three parts: the wireless base station (WBS), the wireless intelliducer node (node), and the sensors. The WBS is the central communication hub and bridges the gap between the PC software and the sensors. It refers to the combined unit of the actual base station mounted to a tripod along with a router for wireless capabilities. This mounting configuration allows for easier travel and a stronger signal. Each node provides four channels for sensors to be connected simultaneously. Once sensors are connected, the node passes along the data to the WBS which then sends it to the PC running the STS Live software. This project utilized two types of sensors- the strain gauge and the accelerometer.

Figure 6.1.1: Wireless Base Station mounted on tripod with Router

Figure 6.1.2: Wireless Intelliducer Node

6.1.1 Strain Gauge

The ST350 Strain Transducer (strain gauge) is a reusable sensor that measures live-load strain on any structure. As seen in the figure below, the strain gauge has two openings which allow small mounts to be secured with a nut and bolt. Rather than the sensor itself being attached to a structure, the two mounts are aligned and tightened to the sensor and then attached to the structure. The sensor can then be applied using specifically Loctite 444 adhesive alongside Loctite 7452 accelerator. This combination is recommended by BDI for use with the sensors as it quickly creates a reliable bond between the sensor and the structure which is important for receiving reliable data. The sensor should be placed along the axis which is expected to experience the most amount of strain.

Figure 6.2.1: ST350 Strain Transducer

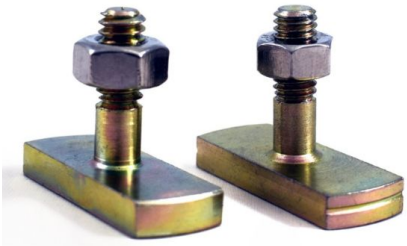

Figure 6.2.2: Sensor Mounting Tabs

Figure 6.2.3: Tab Jig for Aligning Mounting Tabs

6.1.2 Accelerometer

The UA1512 Uniaxial Accelerometer (accelerometer) is a reusable sensor that measures vibrations on any structure. Like the strain gauge, it also is applied using Loctite 444 adhesive and Loctite 7452 accelerator. Due to its small size, however, it only requires one mount to be secured. It is recommended to be used from zero to medium frequency applications. A biaxial and triaxial model of the accelerometer are available, but since this model is uniaxial, it is important to place the accelerometer on the axis of most interest.

Figure 6.3: UA1512 Uniaxial Accelerometer

6.1.3 STS Live by BDI

STS Live is the software engineered by BDI to collect and display the data being collected from the sensors. It is important to be just as familiar with the software as with the sensors because many important features of the sensors must be configured in the software such as sample frequency and test duration. Additionally, the software displays the data in real time as it is received which allows for detection of error or general monitoring.

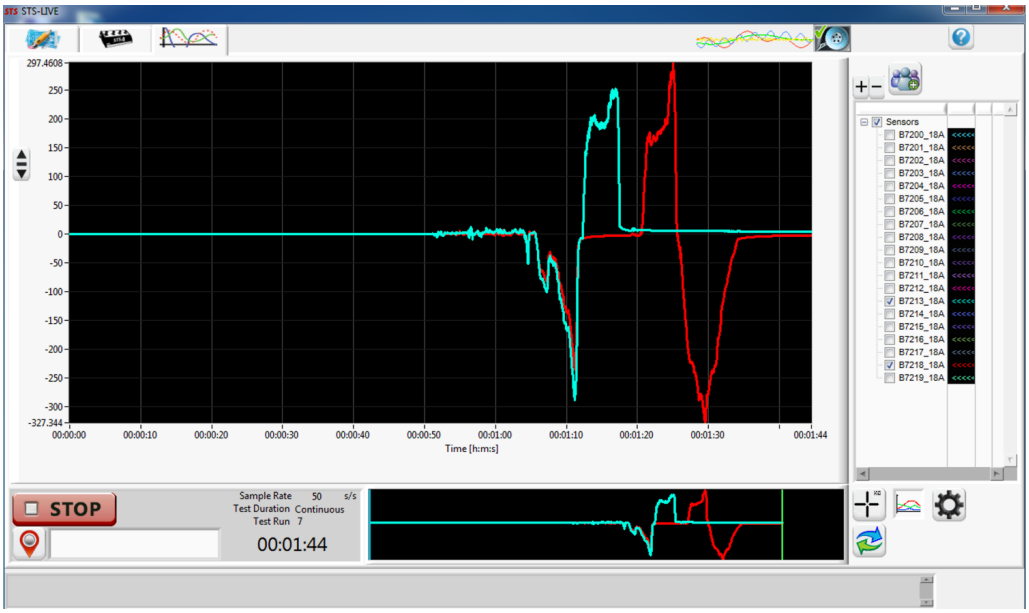

Figure 6.4: Example Window in STS Live

6.2 Moving Load Sensor Test

6.2.1 Test Setup

The moving load test was conducted on the middle three stringers closest to the Indiana side due to their accessibility. A strain sensor was applied on the flange of each stringer using the recommended adhesive. Facing the Indiana approach, the strain sensor on the left stringer (B7754) was denoted as "Left." The strain sensor on the middle stringer (B7753) was denoted as "Middle." The strain sensor on the right stringer (B7756) was denoted as "Right."

Figure 6.5: Map for Sensor Placement

Figure 6.6.1: Strain Sensor Applied to Stringer

Figure 6.6.2: Strain Sensor Applied to Stringer

6.2.2 Procedure

The procedure for the moving load test was quite simple. Both Scales and Butler walked along the beam until they were directly above the sensor, waited three seconds, jumped, waited another three seconds, then walked the opposite way along the beam. This was repeated for each of the three sensors, resulting in three separate data sets. This specific procedure was developed in order to induce three different types of loading for each test. At the beginning of the test, there is essentially no loading since Scales and Butler are too far for the sensors to recognize. Once they begin to approach, however, a moving load is being applied as they walk nearer to the sensor and eventually stop directly above. The readings then stabilize for those three seconds of standing still, followed by a point load during the jump. This provides variation in the loading that can be seen graphically as well.

6.3 Data and Results

Each of the three tests display strain measurements with respect to time graphically for the left, middle and right sensors. These measurements can be used to numerically approximate the fraction of the total load experienced by each sensor's corresponding floor beam.

6.3.1 "Left" Sensor Test Results

The "Left" Sensor Test is the test that was performed over the "Left" sensor. Figure 6.7 displays the raw data without any alterations. The x-axis displays time while the y-axis displays the strain measurements in units of microstrain. The left sensor is shown in blue, the middle in green, and the right in red as denoted by the legend. The entire test only lasted around one minute.

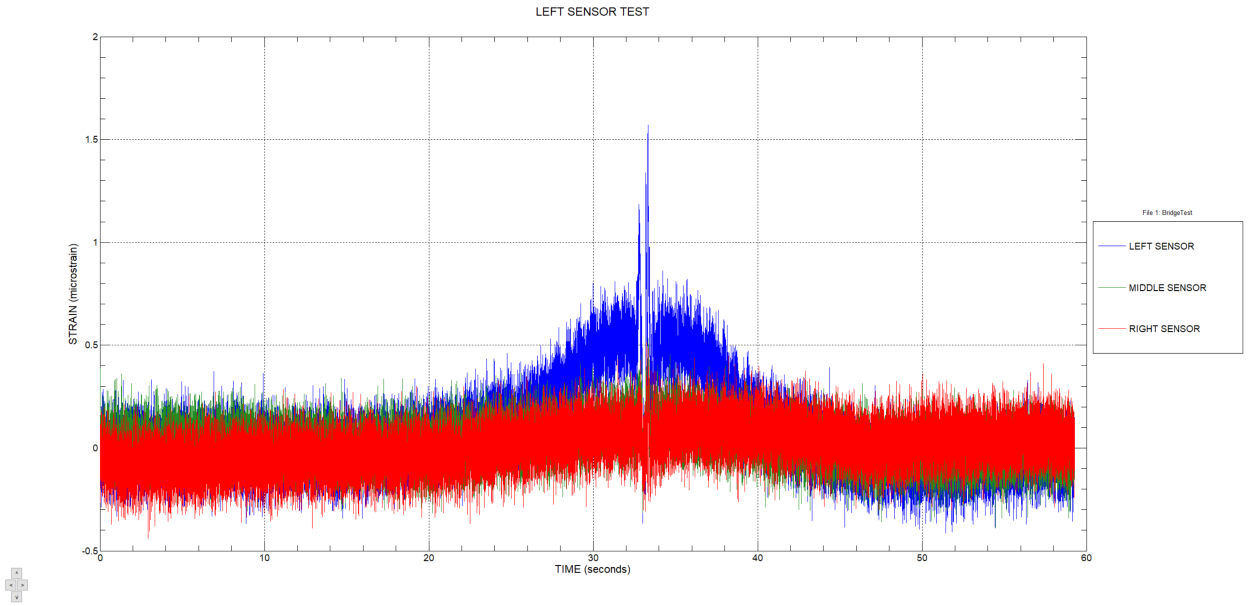

Figure 6.7: Raw Data for Left Sensor Test

This data was then filtered in order to reduce noise and more clearly define the average. The boxcar method was used with a factor of 0.01 to produce the graph shown in Figure 6.8. This figure also displays the breakdown of loading scenarios present during the test. For the first twenty seconds of the test, essentially no loading occurred. For the next ten seconds, the moving load can be seen visually as the strain trends upward.

Finally, the point load occurs at the thirty second mark.

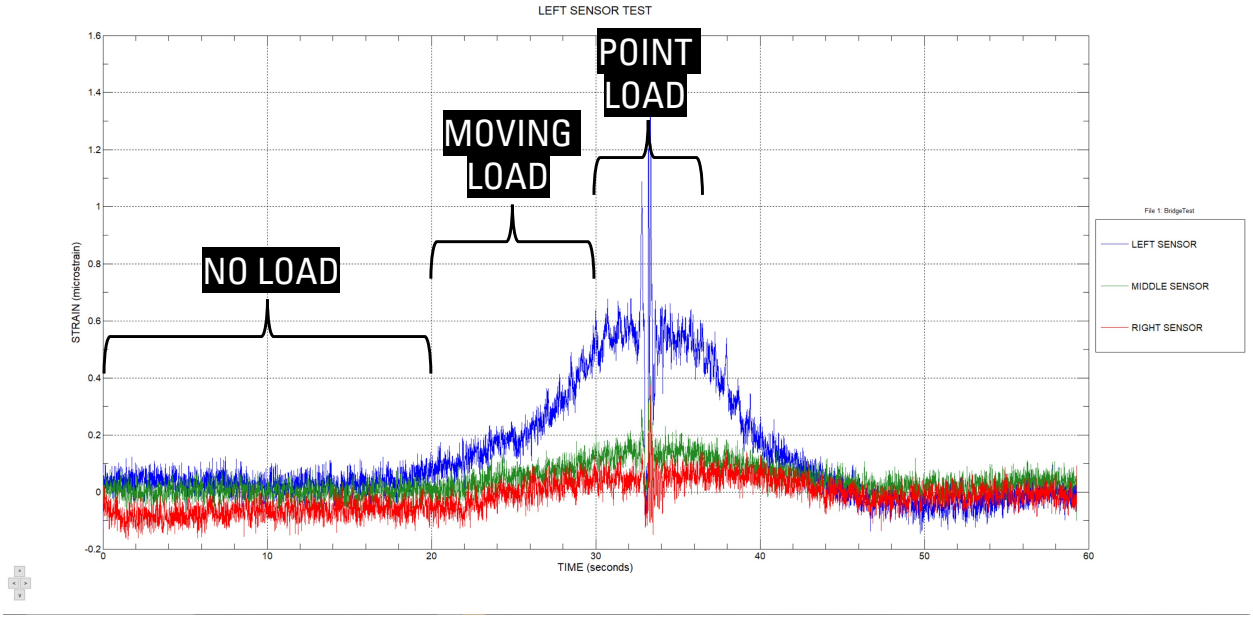

Figure 6.8: Filtered Data for Left Sensor Test

The point load section of the data can then be magnified in order to compare strain measurements among the three sensors. For the left sensor, microstrain measured approximately 0.5, while the two remaining sensors measured approximately 0.1. By simply dividing the microstrain reading of the sensor being tested by the total microstrain readings among all three sensors, a percentage of load sharing can be calculated. In this case, the left sensor is experiencing 5/7 of the load that is being applied. This is evident of little load sharing since the left sensor is bearing the majority of the load rather than evenly dispersing it among neighboring beams.

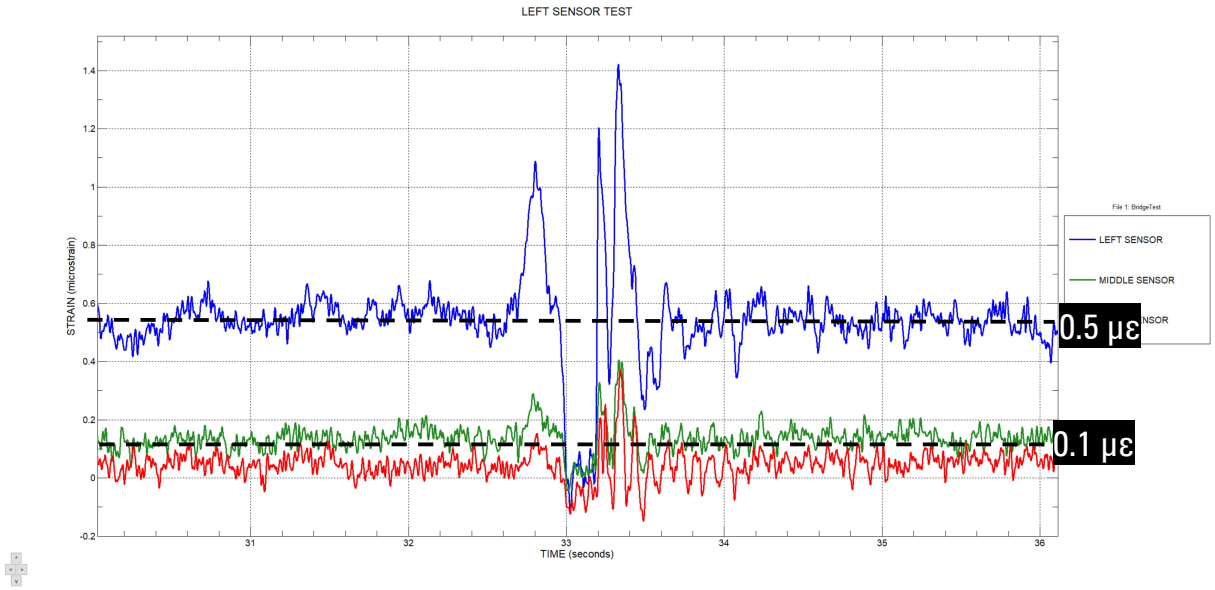

Figure 6.9: Left Sensor Test Data Magnified at Point Load

6.3.2 "Middle" Sensor Test Results

An identical approach is used for all tests to analyze load sharing capabilities. Figure 6.10.1 displays the filtered test data after the boxcar filtering approach was applied. Figure 6.10.2 displays the point load scenario magnified. In this test, all sensors are approximately even in measures of microstrain. Using the same method as was used for the left sensor test, all beams are experiencing approximately a third of the loading. This indicates complete load sharing because the load is dispersed evenly among the beams.

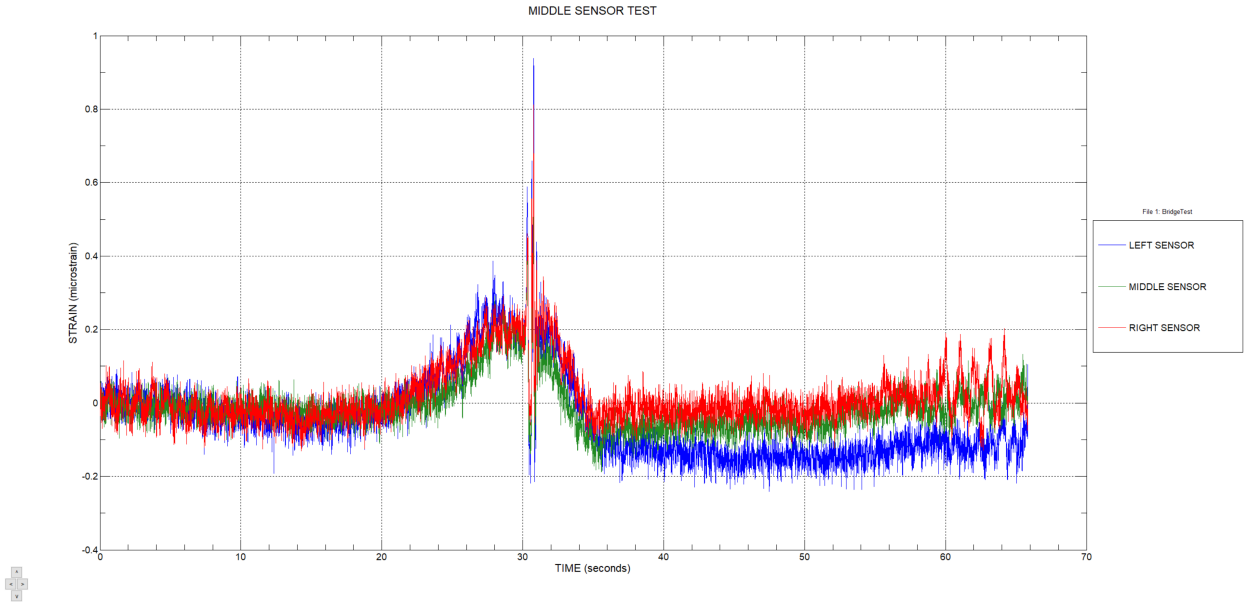

Figure 6.10.1: Middle Sensor Test Filtered Data

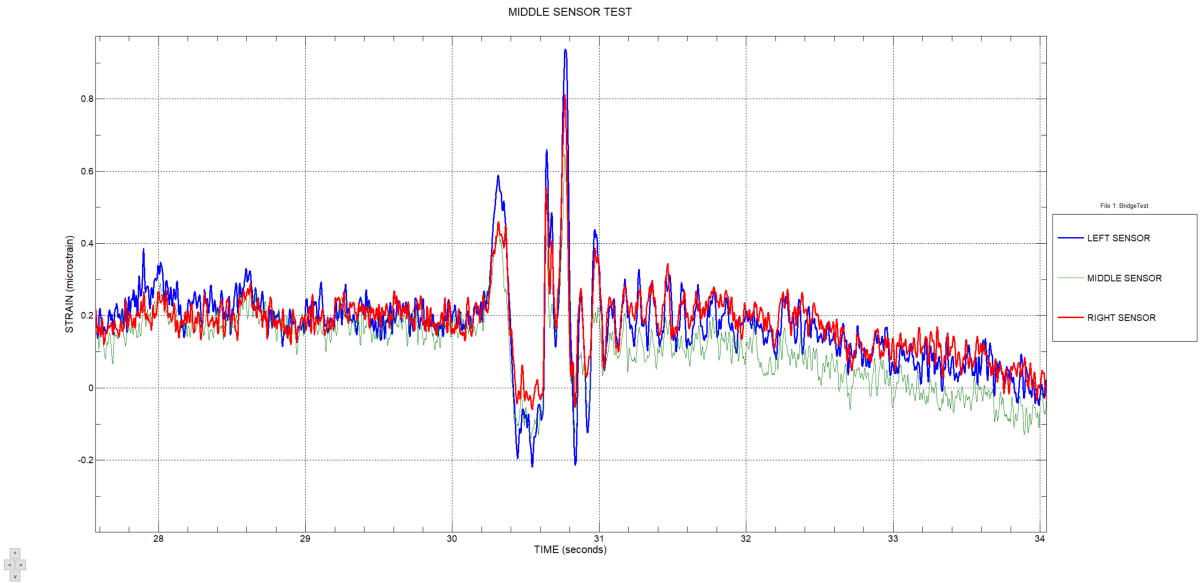

Figure 6.10.2: Middle Sensor Test Magnified at Point Load

6.3.3 "Right" Sensor Test Results

An identical approach is used for all tests to analyze load sharing capabilities. Figure 6.11.1 displays the filtered test data after the boxcar filtering approach was applied. Figure 6.11.2 displays the point load scenario magnified. The right sensor experiences approximately 0.2 microstrain. The middle sensor experiences approximately 0.15 microstrain. The left sensor experiences approximately 0.1 microstrain. Using the same method as was used for the left and middle sensor test, the right beam bears approximately 4/9 of the loading. This is evident of some load sharing. It is not complete load sharing since all sensors do not read the same microstrain value nor is it zero load sharing since every sensor experienced strain.

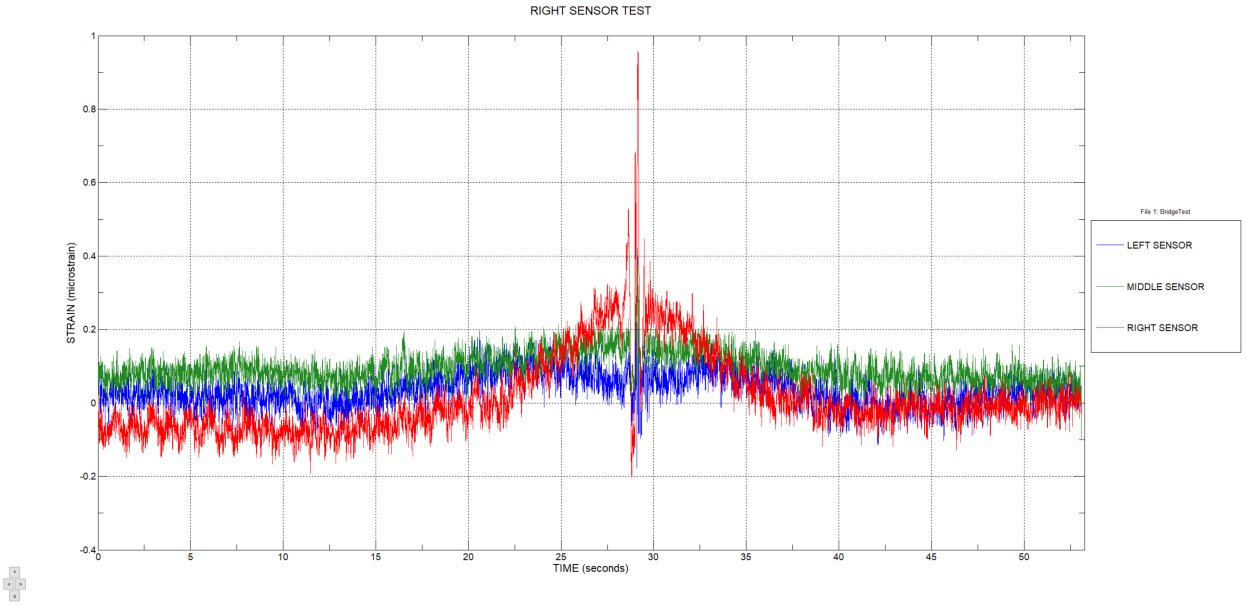

Figure 6.11.1: Right Sensor Test Filtered Data

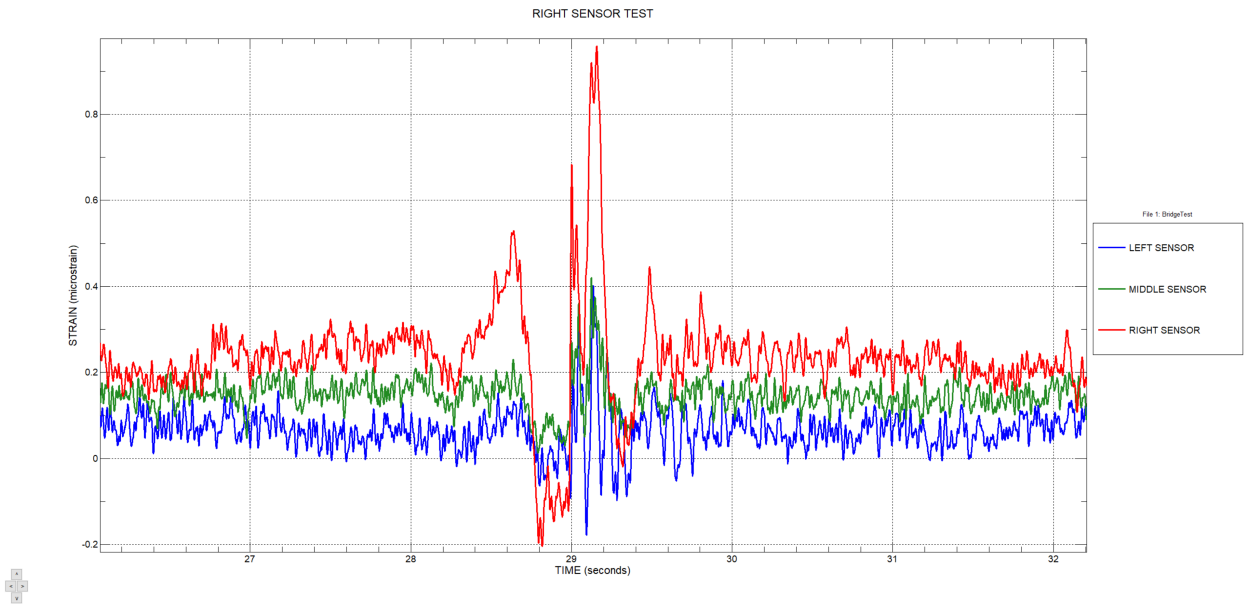

Figure 6.11.2 : Right Sensor Test Magnified at Point Load

7.0 RESULTS AND CONCLUSION

By selecting a composite beam design, the existing capacity improves in the beam significantly and meets AASHTO HS-20. Since the concrete deck was going to be replaced due to significant deterioration, a concrete deck design that also met the HS-20 demand was needed as well. By selecting the same depth as the original deck as 7 inches, a cage design that meets the AASHTO spacing standards and necessary capacity was met. The AASHTO Demands were 38.3 k-ft for the concrete and 530.3 k-ft for the composite beam. The new design attained a minimum moment of 129k-ft for the concrete deck and 538.3 k-ft for the composite beam. The AASHTO demands included amplification factors which increased the overall demand, while AISC featured safety factors that limited the minimum. While the load was not completely shared on the STS testing, each case did share some loading. With load sharing being evident in each of the interior beams, it signifies that the factored capacities met are competent in the new design.

REFERENCES

American Association of State Highway and Traffic Officials. (2012). *AASHTO LRFD Bridge Design Specifications, 6th Edition*

American Concrete institution. (2019) *Building Code requirements for Structural Concrete (ACI 318-19).* ACI.391-401.

American Institute of Steel Construction. (2019) *Steel Construction Manual.* AISC. 3-203, 16.1-105.

Csernak , S & McCormac, J. (2012). *Structural Steel Design 5th Edition*. Pearson. 563-575.

Muhit , Imrose B. Shear Connectors between Concrete Slabs in a Composite Beam Fig 1 (2015). Retreieved From *.researchgate.net%2Ffigure%2FShear-connectors-between-concrete-slabs-and-steel-beams-in-a-composite-beam_fig1_275340980*

K Truss, Pratt Truss. (2021) Retrieved From *https://skyciv.com/docs/tutorials/truss-tutorials/types-of-truss-structures/#warren*

Appendix A: Diagrams of Pratt and K-Trusses, courtesy of Skyciv Civil Engineering

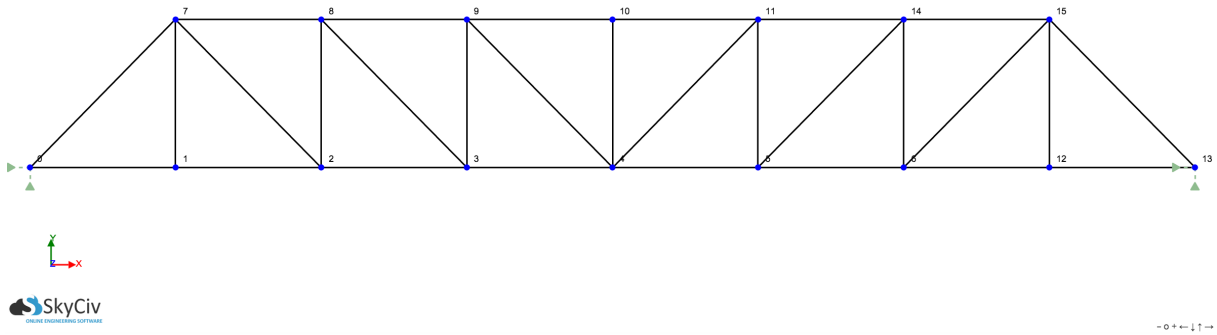

Image A.1: Pratt Truss

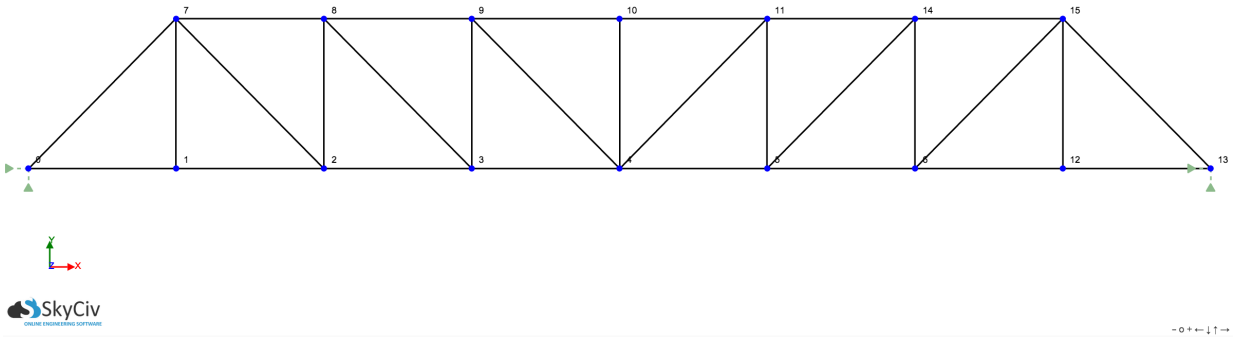

Image A.2: K-Truss

Appendix B: Effective Bases for Interior Beams

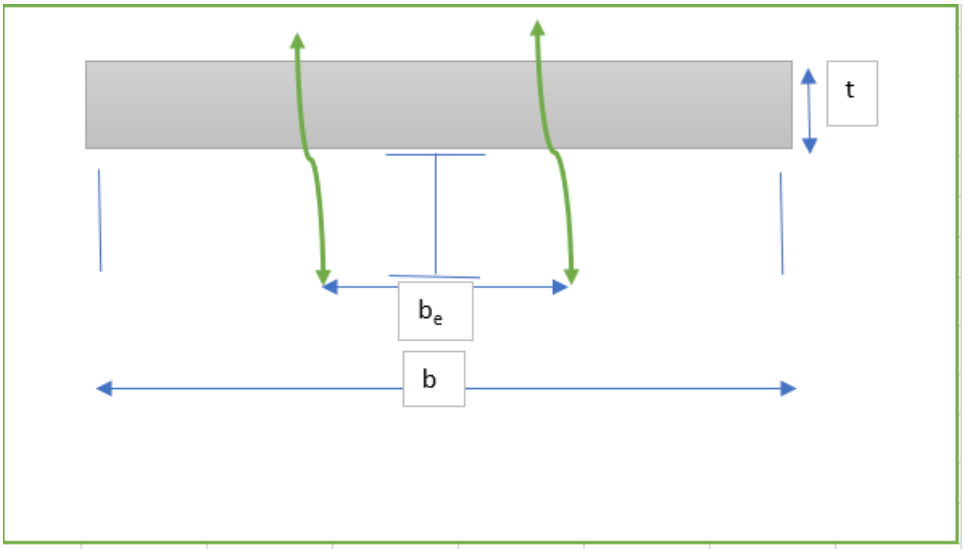

Figure B.1: Effective Base for Interior Beams

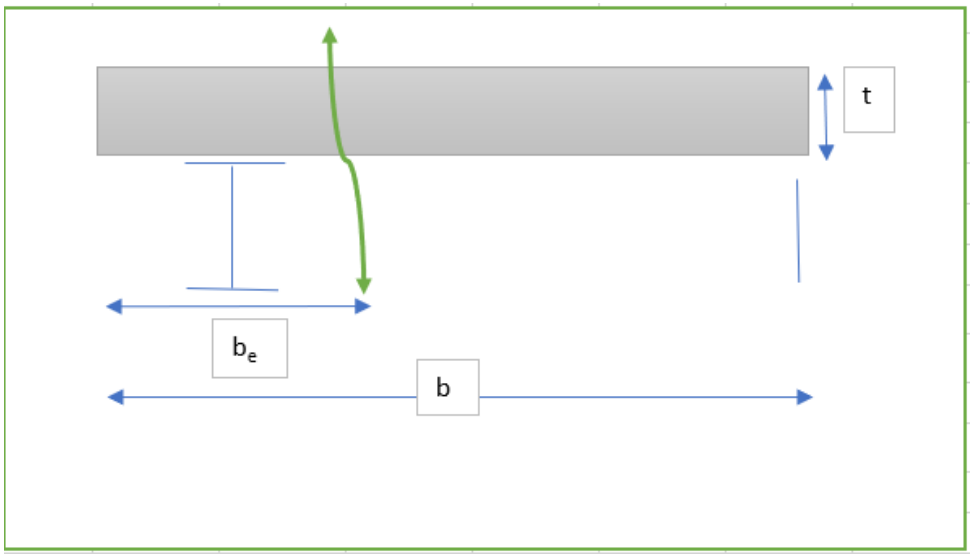

Figure B.2: Effective Base for Exterior Beams

Appendix C: List of Materials

Shear Studs. 5/8” diameter (28 studs per span)

Reinforcement Steel Bars, 5 Gr. 60 Bars (108 bars per span)

Concrete (4000 psi, 7” design depth)

Profiled Sheet Metal, A36 grade (20’x 40’ required per span)

Appendix E: Aides for Composite Design

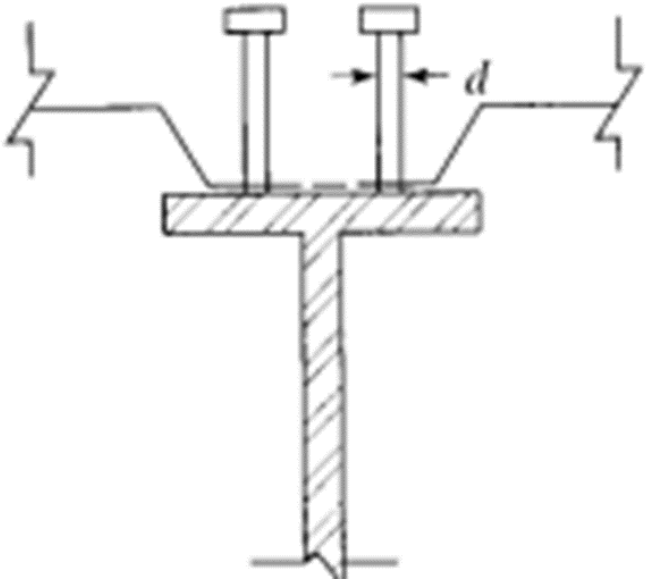

Figure E.1: Steel Beam with Shear Studs (*Structural Steel Design)*

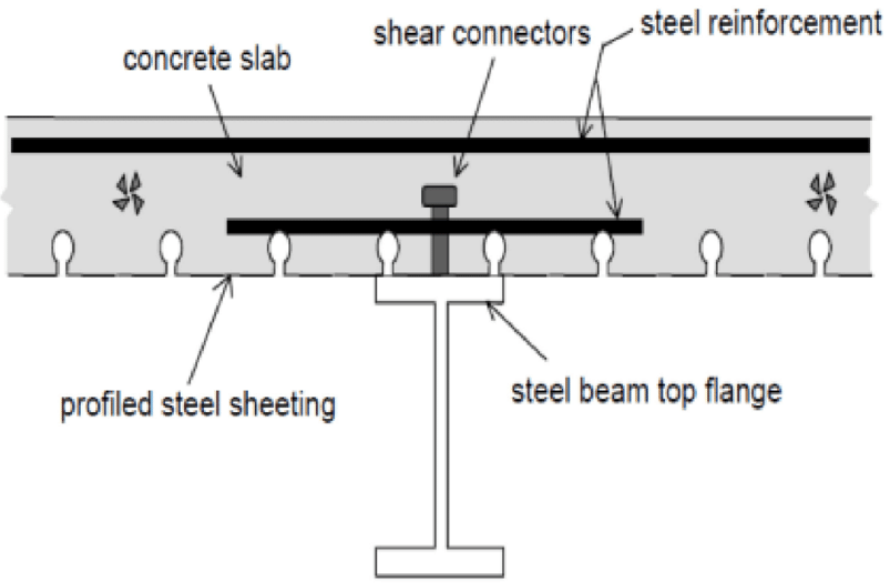

Figure E.2: Diagram including stringer, Shear Studs, and Top and Bottom Steel *(ResearchGate.net)*